Resistive switching in FTO/CuO–Cu_2O/Au memory devices

Amir Shariffar ✉, *Haider Salman, Tanveer A. Siddique, Wafaa Gebril, Mahmoud Omar Manasreh*

Department of Electrical Engineering, University of Arkansas, Fayetteville 72703, USA
✉ *E-mail: ashariff@uark.edu*

Published in Micro & Nano Letters; Received on 14th May 2020; Revised on 11th June 2020; Accepted on 22nd June 2020

Memristors are considered to be next-generation non-volatile memory devices owing to their fast switching and low power consumption. Metal oxide memristors have been extensively investigated and reported to be promising devices, although they still suffer from poor stability and laborious fabrication process. Herein, the authors report a stable and power-efficient memristor with novel heterogeneous electrodes structure and facile fabrication based on cupric oxide (CuO)–cuprous oxide (Cu_2O) complex thin films. The proposed structure of the memristor contains an active complex layer of CuO and Cu_2O sandwiched between fluorine-doped tin oxide (FTO) and gold (Au) electrodes. The fabricated memristors demonstrate bipolar resistive switching (RS) behaviour with a low working voltage (~1 V), efficient power consumption, and high endurance over 100 switching cycles. The authors suggest the RS mechanism of the proposed device is related to the formation and rupture of conducting filaments inside the memristor. Moreover, they analyse the conduction mechanism and electron transport in the active layer of the device during the RS process. Such a facile fabricated device has a promising potential for future memristive applications.

1. Introduction: The memristor (memory + resistor) was first proposed by Leon Chua in 1971 as the fourth fundamental circuit element [1]. A typical structure of two-terminal memristors consists of a switching layer sandwiched between two metallic electrodes. Depending on the switching layer properties, memristors are classified as bulk, interface, and filament types. The filament type memristors continue to attract more research attention due to their superior performance. Among filament types memristors, metal oxides are the most commonly used materials in which oxygen vacancies form conductive filaments that are responsible for resistive switching (RS) behaviour [2]. There have been several studies on metal-oxide memristors such as TiO_2 [3], HfO_2 [4], ZnO [5], AlO_x [6], WO_x [7], TaO_x [8], and so on. Moreover, cupric oxide (CuO) has been also reported to show bipolar memristive behaviour [9–11]. In copper oxide memristors, the active layer is often made by thermal annealing [12], or solution processing [13], which features inexpensive and low-power operation [14]. The facile fabrication of copper oxide memristors is an advantage over other types of metal oxide memristors; however, further efforts are required to improve the stability, endurance, and retention time during the RS mechanism [15, 16]. In this work, we report a stable and power-efficient memristor with novel structure and facile fabrication based on CuO–Cu_2O (cuprous oxide) complex thin films. The fabricated memristor consists of CuO–Cu_2O complex thin films as a switching layer, which is sandwiched between fluorine-doped tin oxide (FTO) and deposited gold (Au) electrodes. The FTO as the bottom electrode acts as an oxygen vacancy reservoir where oxygen vacancies can be stored or supplied during the RS [17]. Moreover, FTO can tolerate high annealing temperature without increasing the sheet resistance during copper (Cu) oxidisation [18]. Au electrodes are deposited on top of the device because compared to platinum (Pt) the Au contact is less expensive and demonstrates higher endurance [19]. Structural and memristive properties are characterised using Raman spectroscopy, UV–Vis absorbance, and current–voltage (I–V) measurements. The memristivity is identified by the pinch hysteresis loop and switching cycles from the high resistance state (HRS) to the low resistance state (LRS). The memristor possesses a low operation voltage, high endurance, and uniformity. Moreover, the carrier transport mechanisms have been investigated, suggesting the space charge limited conduction (SCLC) to be the main conduction mechanism.

2. Fabrication and experimental methods: A 100 nm-thick Cu thin film was deposited on the FTO substrate using electron beam evaporation at room temperature. The vacuum pressure was kept at 6×10^{-6} Torr during the deposition process. The as-deposited Cu metal film was annealed at 400°C for 45 min in an oxygen ambient environment to form the copper oxide thin film. We used Horiba LabRam micro-Raman spectrometer and Cary 500 UV–Vis–NIR spectrophotometer to characterise the Raman and absorbance properties of the thin film, respectively. The Raman measurements are performed using a continuous red (632 nm) laser as the excitation source. The elastically scattered light is filtered out to detect the weaker inelastically scattered light from optical phonons. The Raman spectrum is recorded in the range of 200–700 cm^{-1} to confirm the presence of copper oxide elements by comparing the position of phonon modes with existing literature. We also measured the absorbance of the grown thin films in the wavelength range of 300–800 nm, where the excitonic peak and bandgap of the copper oxide can be observed. To achieve FTO/CuO–Cu_2O/Au devices, the 50 nm-thick circle Au electrodes with different areas were deposited using a shadow mask and electron beam evaporation. We used the Keithley 4200 SCS parameter analyser and a probe station for the I–V characterisation of fabricated devices. For each device on the sample, we applied the consecutive external DC voltages with different polarities between the Au and FTO as top and bottom electrodes. All the measurements were performed at room temperature.

3. Results and discussions: Fig. 1 plots the Raman scattering spectra of the grown copper oxide thin film. The three peaks at 307, 355 and 640 cm^{-1} are the Raman fingerprints of CuO, which is consistent with relevant studies [20, 21]. These strong peaks are assigned to A_g, B_g, and $2B_g$ phonon modes, which can shift slightly depending on the annealing temperature of CuO [22]. There are also broad humps between 390 and 640 cm^{-1}, which indicate the presence of Cu_2O phase [23]. Therefore, the prepared copper oxide thin film contains both CuO and Cu_2O phases. Fig. 2 shows the optical absorption of CuO–Cu_2O complex thin films annealed at 400°C. The thin films exhibit high absorbance in the UV region centred around 350 nm. The inset of Fig. 2 demonstrates the Tauc plot, in which the corresponding bandgap is analysed by extrapolating the linear part of the curve.

© The Institution of Engineering and Technology 2020

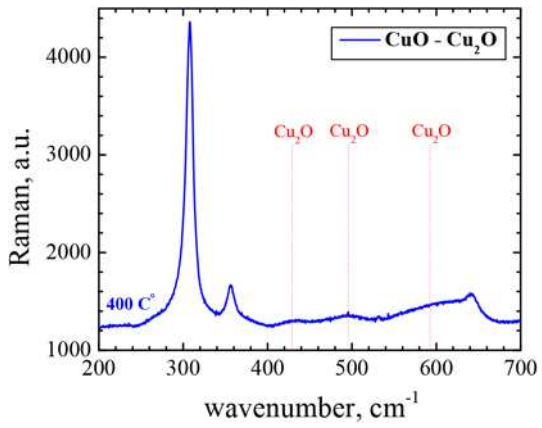

Fig. 1 *Raman scattering spectra of CuO–Cu_2O thin films excited by the red laser*

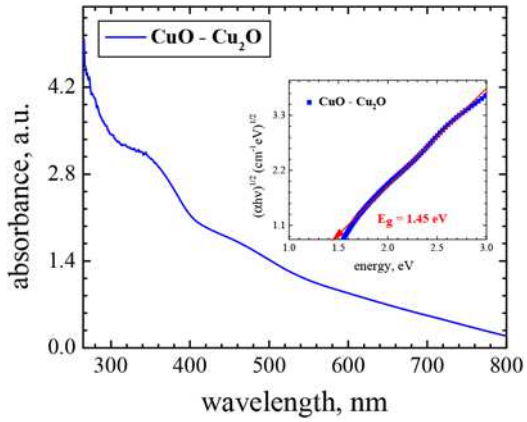

Fig. 2 *Absorbance spectra of CuO–Cu_2O thin films. The inset demonstrates the Tauc plot representing the extrapolation of the linear part of the curve to achieve the indirect bandgap of CuO–Cu_2O thin films*

The obtained indirect bandgap is 1.45 eV that is within the range reported by the authors of [24, 25].

A schematic picture and the structure of two-terminal memory devices studied in this work are shown in Fig. 3*a*. Before performing *I–V* measurements, the electroforming process is required to create a sufficiently strong electric field and initiate a soft breakdown of the switching layer in the device. As a result, massive oxygen vacancies are introduced into the copper oxide layer, which can form nanoscale conductive filaments [26]. To this aim, the applied voltage is slowly increased with a current compliance of 10 mA to protect the device from a permanent breakdown (not shown here). The electroforming process is observed at around −6 V, where the current suddenly increases and stabilises afterwards. Then, when we sweep back the voltage from negative to a positive value with a sweep rate of 10 mV/s, an abrupt current change occurs at ∼3.2 V, indicating RS from an initial LRS to a HRS, which is called the 'RESET' process. Subsequently, we sweep the voltage from positive to a negative value, and the device remains at HRS until another RS occurs around −1 V, and the device switches back from HRS to LRS, which is called the 'SET' process. The memristive behaviour of the device with the smallest electrode's diameter of 0.2 mm can be observed from the measured *I–V* characteristics shown in Fig. 3*b*. We prepared multiple devices with different Au electrode areas, and the device with the smallest diameter of 0.2 mm exhibits the best performance. Devices with the larger Au electrode areas demonstrate poor performance in terms of endurance, retention

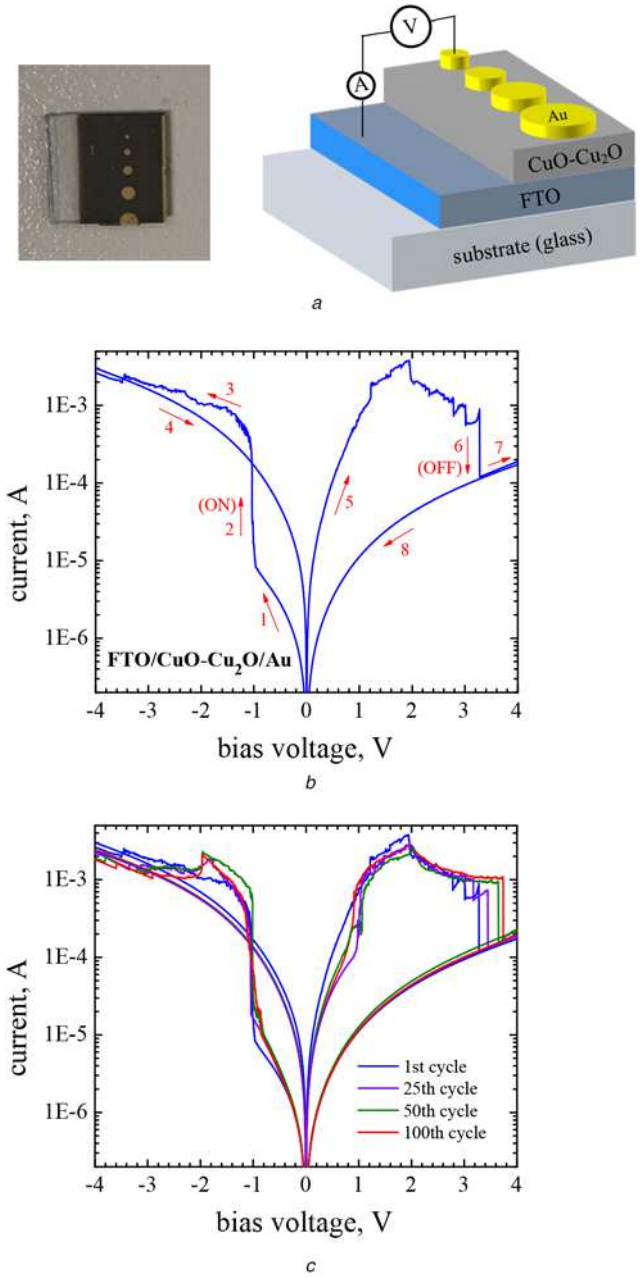

Fig. 3 *FTO/CuO–Cu_2O/Au I–V characteristics*
a Schematic picture (left) and the structure of the fabricated devices (right)
b Typical RS behaviour of the FTO/CuO–Cu_2O/Au device, where arrows indicating the RS operation cycle with ON and OFF switching
c *I–V* characteristics at consecutive switching cycles

time, and on/off ratio. A possible reason can be related to the local RS in the device due to the formation of highly localised filaments [27]. As we expected, the *I–V* characteristics are asymmetric, which can be used to differentiate similar conduction mechanisms from each other [28]. By sweeping voltage repeatedly between positive and negative values, the *I–V* curves show little difference between first and last sweeping cycles, indicating high endurance and reproducibility up to 100 cycling times (Fig. 3*c*). Thus, the RS behaviour is reversible and instantaneous, which is important for a reliable non-volatile memory mechanism. However, the origin of RS mechanism is still in debate, relevant studies on copper oxide based devices agree on the formation and rupture of conducting filaments with oxygen vacancies accumulation and depletion induced by applying the external voltage [29]. The scattered switching voltage distribution observed at OFF

© The Institution of Engineering and Technology 2020

doi: 10.1049/mnl.2020.0300

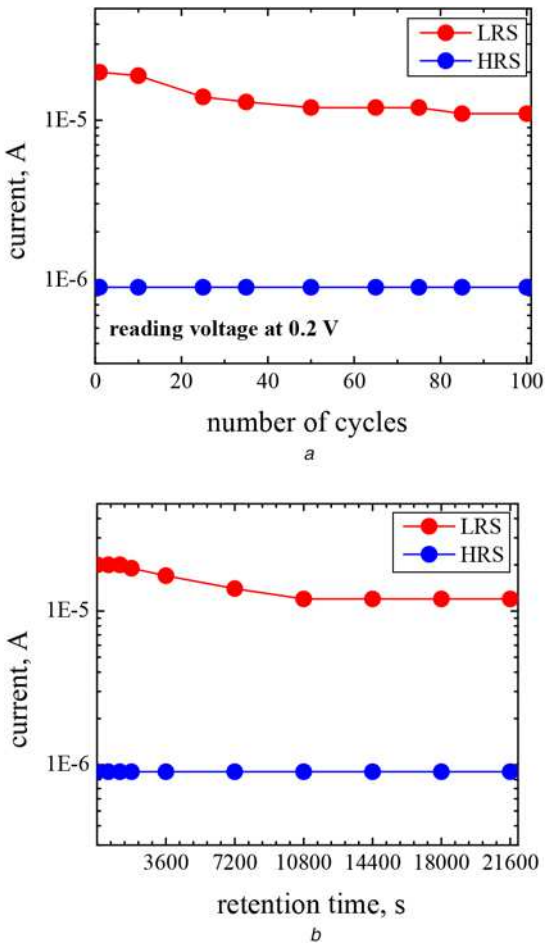

Fig. 4 *Endurance and retention stability performance of the device*
a Endurance performance of the device over 100 consecutive switching cycles
b Retention performance of the device for around 2×10^4 s

states in Fig. 3*c* is due to the rupture of filaments, either by ion migration or Joule heating [30]. Moreover, symmetric multilevel transitions occur at both HRS and LRS states around ±1 V where the possible reason might be the hopping conduction in which the shallow trapped electrons can surpass the energy barrier and form the leakage current in discontinuous residual metallic filament [31]. This phenomenon can also suggest a multilevel data storage capability of the device [32]. Another advantage of this device is low power consumption (<4 μW), which is calculated by multiplying the reading voltage (0.2 V) and LRS current values (<20 μA) [33]. Fig. 4*a* depicts the device endurance performance, in which the current values of LRS and HRS are monitored at 0.2 V. The HRS current state is consistent over 100 cycles, and LRS current also becomes stable after the first several cycles, indicating a good endurance of the device performance.

From the current ratio, the memory window is maintained well at more than one order of magnitude difference thus, we can well distinguish between the binary storage information. The retention characteristic is shown in Fig. 4*b*, which demonstrate continuous sampling for around 2×10^4 s at room temperature. The HRS current state remains consistent while the LRS current decays a little bit after 10^3 s and again maintains consistency around 10 μA. The overall device performance is compared with recent publications in Table 1. To further understand the switching and conduction mechanism of the device, the linear fitting *I–V* characteristics of positive and negative bias regions are plotted on a separate double logarithmic scale (Fig. 5). In the low voltage negative bias region (Fig. 5*a*), the curve's slope is ∼1 for both HRS and LRS states, indicating the Ohmic conduction is dominant at low voltages ($I \propto V$). It means that thermally generated free carriers in the oxide film mainly contribute to the conduction and exceed injected carriers when the applied bias voltage is low. As the negative voltage scans forward, the curve's slope increases to 2, which is following Child's square law ($I \propto V^2$). In the higher field regions, a steep current increase occurs around 1*V* due to the formation of filaments and trapping the injected carriers in the oxide layer where $I \propto V^a$ (a > 2).

For copper oxide thin films, the traps are well known to be as oxygen vacancies. When traps or oxygen vacancies are gradually filled by injected carriers, the slope reduces to around 2 again [30]. Therefore, the fitting results suggest that the conduction mechanism follows the SCLC model. This model is constituted of three regions: (i) Ohmic region, (ii) Child's square law or trap-unfilled SCLC region, and (iii) trap-filled SCLC region. According to the SCLC theory at higher fields or trap-free SCLC region

$$J = \frac{9}{8}\varepsilon\mu\theta\frac{V^2}{d^3}$$

where J is the current density, ε is the permittivity of the oxide layer, μ is the mobility of charge carriers, θ is the ratio between free and shallow trapped charge carriers, and d is the film thickness [35]. In the positive bias region (Fig. 5*b*), a similar conduction mechanism is observed, which obeys the SCLC model. The LRS state with a slope of 1 is still maintained, which is followed by the Child's law with a slope of 2 until the rupture of conductive filament gradually occurs, and the device resets back to HRS.

Based on the above analysis, the RS mechanism is bipolar in which the SET and RESET processes occur in different polarities. The forming or SET process is due to a dielectric soft breakdown in the oxide layer [36], and then oxygen ions (O^{2-}) move through the filament (oxygen vacancies) to the anode as an oxygen vacancy absorber (FTO). At the anode interface, the oxygen ions reoxidise ($O^{2-} = O + 2e^-$), creating an oxygen reservoir [29]. The RESET process occurs at the reverse polarity where oxygen ions

Table 1 Device performance comparison between this work and other publications regarding copper oxide RS

Device structure	Endurance (cycle)	Retention, s	Set/reset, V	Power consumption, W	On/off ratio	$V_{forming}$, V	Fabrication technique	Refs.
FTO/CuO–Cu_2O/Au	>100	$>2 \times 10^4$	−1/+3.2	$<4 \times 10^{-6}$	>10	6	thermal annealing	this work
ITO/Cu_xO/Au	200	$>10^4$	−0.7/+0.7	$<10 \times 10^{-6}$	>10	free	solution processing	[13]
Al/CuO/SS	—	600	+1.8/−1.8	—	—	free	hydrothermal	[9]
Ti/Cu_xO/Pt	100	$>10^2$	+0.8/−1	6×10^{-4}	100	14.8	thermal annealing	[27]
Cu/CuO/AgO/Ag	—	—	−0.8/+0.8	4×10^{-3}	10	free	solution processing	[14]
Cu/CuO/Ag	100	—	+2/−2	—	—	free	thermal annealing	[12]
TiW/Cu_2O/Cu	—	—	+0.55/−0.3	20×10^{-6}	>10	free	DC sputtering	[34]

© The Institution of Engineering and Technology 2020

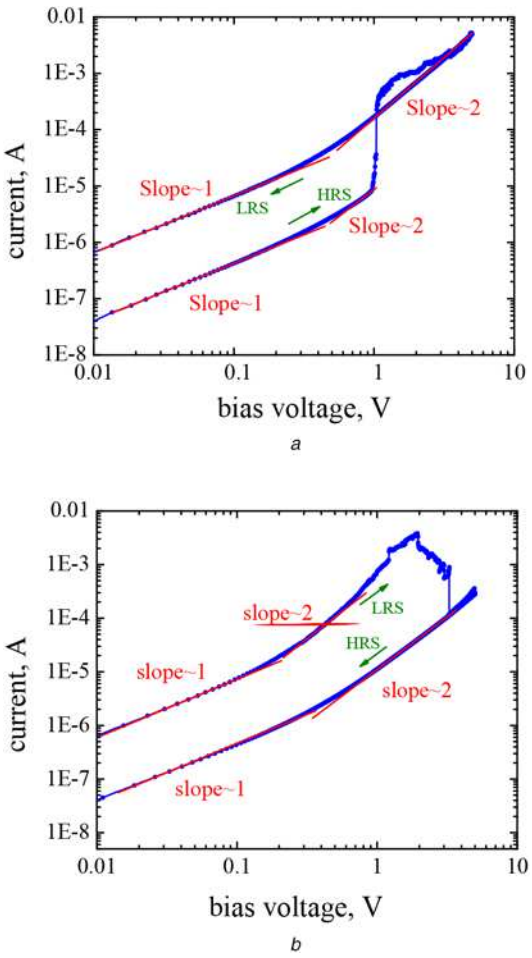

Fig. 5 *Linear fitting I–V characteristics for the double logarithmic plots of Fig. 3b, indicating the corresponding curve's slopes and the conduction mechanism of the device*
a Negative voltage bias region
b Positive voltage bias region

are repelled from the anode interface because they are negatively charged. Therefore, based on the external voltage polarity, the oxygen ions are repelled or extracted back to the anode, switching the device between LRS and HRS states. A detailed explanation of the filamentary switching mechanism remains an area of active research.

4. Conclusion: In summary, we reported a facile fabrication method and analysed the RS behaviour of the heterogeneous electrodes structure of FTO/CuO–Cu_2O/Au memristor. The copper oxide complex layer after annealing is investigated by Raman and absorbance measurements. The conduction mechanism of this device is also investigated, which follows the SCLC theory. The achieved results suggest high endurance, low SET voltage, and efficient power consumption of the device. However, further investigations are required to increase the retention time and on/off ratio in this type of memristor.

5. Acknowledgment: This work was supported by the Graduate Professional Student Congress (GPSC) Research Grant at the University of Arkansas.

6 References

[1] Chua L.: 'Memristor-the missing circuit element', *IEEE Trans. Circuit Theory*, 1971, **18**, (5), pp. 507–519
[2] Sun W., Gao B., Chi M., *ET AL.*: 'Understanding memristive switching via in situ characterization and device modeling', *Nat. Commun.*, 2019, **10**, (1), p. 3453
[3] Strukov D.B., Snider G.S., Stewart D.R., *ET AL.*: 'The missing memristor found', *Nature*, 2008, **453**, (7191), pp. 80–83
[4] Niu G., Calka P., Auf der Maur M., *ET AL.*: 'Geometric conductive filament confinement by nanotips for resistive switching of HfO2-RRAM devices with high performance', *Sci. Rep.*, 2016, **6**, (1), p. 25757
[5] Laurenti M., Porro S., Pirri C.F., *ET AL.*: 'Zinc oxide thin films for memristive devices: a review', *Crit. Rev. Solid State Mater. Sci.*, 2017, **42**, (2), pp. 153–172
[6] Liu C., Wang L.-G., Cao Y.-Q., *ET AL.*: 'Synaptic functions and a memristive mechanism on Pt/AlO_x /HfO_x /Tin bilayer-structure memristors', *J. Phys. Appl. Phys.*, 2020, **53**, (3), p. 035302
[7] Xia Q., Yang J.J.: 'Memristive crossbar arrays for brain-inspired computing', *Nat. Mater.*, 2019, **18**, (4), pp. 309–323
[8] Kim W., Chattopadhyay A., Siemon A., *ET AL.*: 'Multistate memristive tantalum oxide devices for ternary Arithmetic', *Sci. Rep.*, 2016, **6**, (1), p. 36652
[9] Dongale T.D., Pawar P.S., Tikke R.S., *ET AL.*: 'Mimicking the synaptic weights and human forgetting curve using hydrothermally grown nanostructured CuO memristor device', *J. Nanosci. Nanotechnol.*, 2018, **18**, (2), pp. 984–991
[10] Nyenke C., Dong L.: 'Fabrication of a W/CuxO/Cu memristor with sub-micron holes for passive sensing of oxygen', *Microelectron. Eng.*, 2016, **164**, pp. 48–52
[11] Liu H., Liu Y., Guo W., *ET AL.*: 'Laser assisted ink-printing of copper oxide nanoplates for memory device', *Mater. Lett.*, 2020, **261**, p. 127097
[12] Ortega-Reyes L., Ávila-García A.: 'Memristors based on thermal copper oxide', *J. Mater. Sci. Mater. Electron.*, 2020, **31**, pp. 7445–7454
[13] Rehman S., Hur J.-H., Kim D.: 'Resistive switching in solution-processed copper oxide (Cu_xO) by stoichiometry tuning', *J. Phys. Chem. C*, 2018, **122**, (20), pp. 11076–11085
[14] Xu P., Hamilton M.C., Zou S.: 'Resistive switching characteristics in printed Cu/CuO/(AgO)/Ag memristors', *Electron. Lett.*, 2013, **49**, (13), pp. 829–830
[15] Li Y., Long S., Liu Q., *ET AL.*: 'Resistive switching performance improvement via modulating nanoscale conductive filament, involving the application of two-dimensional layered materials', *Small*, 2017, **13**, (35), p. 1604306
[16] Sung C., Hwang H., Yoo I.K.: 'Perspective: A review on memristive hardware for neuromorphic computation', *J. Appl. Phys.*, 2018, **124**, (15), p. 151903
[17] Shi T., Yin X.-B., Yang R., *ET AL.*: 'Pt/WO_3 /FTO memristive devices with recoverable pseudo-electroforming for time-delay switches in neuromorphic computing', *Phys. Chem. Chem. Phys.*, 2016, **18**, (14), pp. 9338–9343
[18] Yang J.K., Liang B., Zhao M.J., *ET AL.*: 'Reference of temperature and time during tempering process for non-stoichiometric FTO films', *Sci. Rep.*, 2015, **5**, (1), p. 15001
[19] Khrapovitskaya Y., Maslova N., Sokolov I., *ET AL.*: 'The titanium oxide memristor contact material's influence on element's cyclic stability to degradation: the titanium oxide memristor contact material's influence on element's cyclic stability to degradation', *Phys. Status Solidi C*, 2015, **12**, (1–2), pp. 202–205
[20] Chen L.-C., Chen C.-C., Liang K.-C., *ET AL.*: 'Nano-structured CuO-Cu2O Complex thin film for application in CH3NH3PbI3 perovskite solar cells', *Nanoscale Res. Lett.*, 2016, **11**, (1), p. 402
[21] Dhineshbabu N.R., Rajendran V., Nithyavathy N., *ET AL.*: 'Study of structural and optical properties of cupric oxide nanoparticles', *Appl. Nanosci.*, 2016, **6**, (6), pp. 933–939
[22] Madelung O.: 'Semiconductors: data handbook' (Springer Science & Business Media, Germany, 2012)
[23] Akgul F.A., Akgul G., Yildirim N., *ET AL.*: 'Influence of thermal annealing on microstructural, morphological, optical properties and surface electronic structure of copper oxide thin films', *Mater. Chem. Phys.*, 2014, **147**, (3), pp. 987–995
[24] Wanjala K.S., Njoroge W.K., Makori N.E., *ET AL.*: 'Optical and electrical characterization of CuO thin films as absorber material for solar cell applications', *Am. J. Condens. Matter Phys.*, 2016, **6**, (1), pp. 1–6
[25] Zheng W., Chen Y., Peng X., *ET AL.*: 'The phase evolution and physical properties of binary copper oxide thin films prepared by reactive magnetron sputtering', *Mater. Basel Switz.*, 2018, **11**, (7), p. 1253

© The Institution of Engineering and Technology 2020

doi: 10.1049/mnl.2020.0300

[26] Wang T., Shi Y., Puglisi F.M., *ET AL.*: 'Electroforming in metal-oxide memristive synapses', *ACS Appl. Mater. Interfaces*, 2020, **12**, (10), pp. 11806–11814
[27] Wang S.-Y., Huang C.-W., Lee D.-Y., *ET AL.*: 'Multilevel resistive switching in Ti/CuxO/Pt memory devices', *J. Appl. Phys.*, 2010, **108**, (11), p. 114110
[28] Huang J.-J., Kuo C.-W., Chang W.-C., *ET AL.*: 'Transition of stable rectification to resistive-switching in Ti/TiO2/Pt oxide diode', *Appl. Phys. Lett.*, 2010, **96**, (26), p. 262901
[29] Wong H.-S.P., Lee H.-Y., Yu S., *ET AL.*: 'Metal–oxide RRAM', *Proc. IEEE*, 2012, **100**, (6), pp. 1951–1970
[30] Zhu Y.B., Zheng K., Wu X., *ET AL.*: 'Enhanced stability of filament-type resistive switching by interface engineering', *Sci. Rep.*, 2017, **7**, (1), p. 43664
[31] Chen K.-H., Chang K.-C., Chang T.-C., *ET AL.*: 'Effect of different constant compliance current for hopping conduction distance properties of the Sn:SiOx thin film RRAM devices', *Appl. Phys. A*, 2016, **122**, (3), p. 228
[32] Yang Y.C., Pan F., Liu Q., *ET AL.*: 'Fully room-temperature-fabricated nonvolatile resistive memory for ultrafast and high-density memory application', *Nano Lett.*, 2009, **9**, (4), pp. 1636–1643
[33] Fan Y.-S., Liu P.-T.: 'Characteristic evolution from rectifier Schottky diode to resistive-switching memory with Al-doped zinc tin oxide film', *IEEE Trans. Electron Devices*, 2014, **61**, (4), pp. 1071–1076
[34] Yan P., Li Y., Hui Y.J., *ET AL.*: 'Conducting mechanisms of forming-free Tiw/Cu_2O/Cu memristive devices', *Appl. Phys. Lett.*, 2015, **107**, (8), p. 083501
[35] Lampert M.A., Schilling R.B.: 'Chapter 1 current injection in solids: the regional approximation method', in: 'Semiconductors and semimetals' (Elsevier, USA, 1970), pp. 1–96
[36] Xu N., Liu L., Sun X., *ET AL.*: 'Characteristics and mechanism of conduction/set process in TiN/ZnO/Pt resistance switching random-access memories', *Appl. Phys. Lett.*, 2008, **92**, (23), p. 232112

© The Institution of Engineering and Technology 2020